Discovery of a low-temperature orthorhombic phase of the $Cd_2Re_2O_7$ superconductor

Konrad J. Kapcia[1,*] Maureen Reedyk[2] Mojtaba Hajialamdari[2] Andrzej Ptok[1] Przemysław Piekarz[1] Armin Schulz[3] Fereidoon S. Razavi[2] Reinhard K. Kremer[3,†] and Andrzej M. Oleś[3,4,‡]

[1]*Institute of Nuclear Physics, Polish Academy of Sciences, W. E. Radzikowskiego 152, 31342 Kraków, Poland*

[2]*Department of Physics, Brock University, St. Catharines, Ontario, Canada L2S 3A1*

[3]*Max Planck Institute for Solid State Research, Heisenbergstrasse 1, 70569 Stuttgart, Germany*

[4]*Institute of Theoretical Physics, Jagiellonian University, Profesora Stanisława Łojasiewicza 11, 30348 Kraków, Poland*

(Received 31 March 2020; revised 19 June 2020; accepted 24 June 2020; published 21 July 2020)

The favorable combination of Raman spectroscopy of the lattice vibrations with *ab initio* phonon calculations enables us to pinpoint a low-temperature orthorhombic phase which hosts the cryptic 1 K superconducting phase of the 5*d* pyrochlore-type superconductor $Cd_2Re_2O_7$. Raman studies are performed on crystals with the natural isotope abundance and cadmium and oxygen isotope enriched samples. Characteristic splitting and the appearance of sharp phonon modes in the temperature-dependent Raman spectra prove a structural phase below ∼80 K, induced by a soft-mode phonon instability of the intermediate-temperature tetragonal crystal structure. The theory predicts that this low-temperature orthorhombic crystal structure is described by the space group $F222$; it exhibits no phonon instabilities and has the lowest total energy. Future experiments on the $F222$ phase should establish whether spin-triplet components contribute to the superconducting phase.

DOI: 10.1103/PhysRevResearch.2.033108

I. INTRODUCTION

Superconductivity in materials with noncentrosymmetric crystal structures currently attracts broad attention [1,2]. When parity is not a good quantum number anymore, antisymmetric spin-orbit coupling may mix spin-singlet with spin-triplet components within the superconducting (SC) phase [3], and as a result odd-parity and even-parity order parameters coexist [4]. Materials containing heavy 4*d* (5*d*) transition-metal elements with strong spin-orbit coupling are especially promising candidates to search for such states [5]. Strong spin-orbit coupling in a correlated electron system can realize an unconventional ground state of quantum matter, as pointed out recently [6,7]. The ternary oxide $Cd_2Re_2O_7$ (CRO) containing the 5*d* transition metal Re is the first discovered pyrochlore oxide superconductor with $T_c \simeq 1$ K [8–10].

Among a number of unusual properties reported for CRO, a series of structural phase transitions (SPTs) is of particular interest since it essentially determines the low-temperature (LT) structural and electronic properties [11]. In order to understand the character of the SC state, we focus on the characterization of the crystal structure at the lowest temperatures. At room temperature (RT) CRO crystallizes in a cubic structure (phase I, $Fd\bar{3}m$, No. 227). By lowering temperature, a second-order SPT to a noncentrosymmetric tetragonal structure (phase II, $I\bar{4}m2$, No. 119) takes place at ∼200 K as well as a subsequent first-order SPT at ∼120 K to another noncentrosymmetric tetragonal structure (phase III, $I4_122$, No. 98) [12,13] (see Fig. 1). So far, it is common belief that superconductivity occurs in this latter phase.

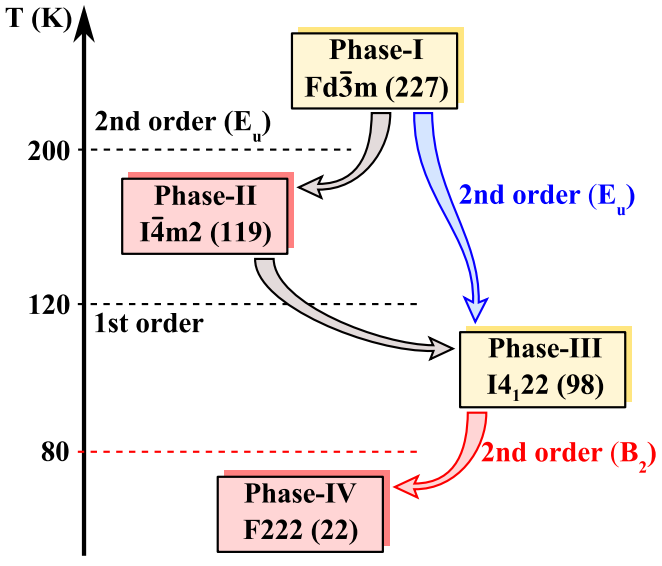

FIG. 1. Different phases of $Cd_2Re_2O_7$ found in DFT calculations. Red and gray arrows denote the structural phase transitions observed experimentally. For the second-order SPTs, the irreducible representations of the associated soft modes are indicated. Red (yellow) boxes denote dynamically stable (unstable) phases in our *ab initio* phonon studies.

*konrad.kapcia@ifj.edu.pl
†rekre@fkf.mpg.de
‡Corresponding author: a.m.oles@fkf.mpg.de

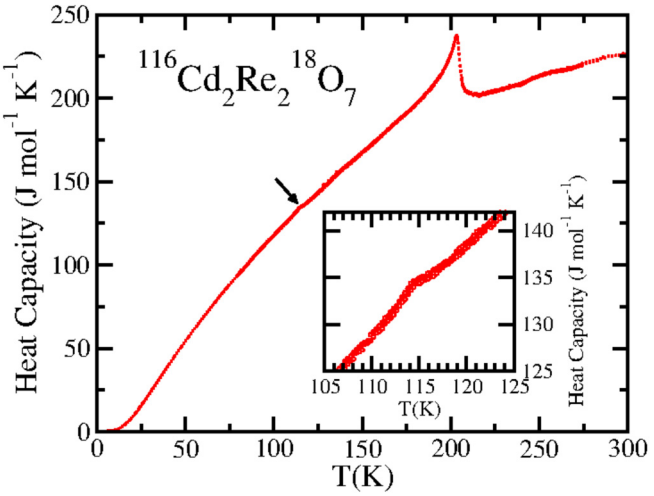

FIG. 2. Specific-heat capacity of a crystal of the isotope enriched material $^{116}Cd_2Re_2^{18}O_7$. Anomalies at ∼204 K and at ∼114 K indicate the SPT from phase I to phase II and from phase II to phase III.

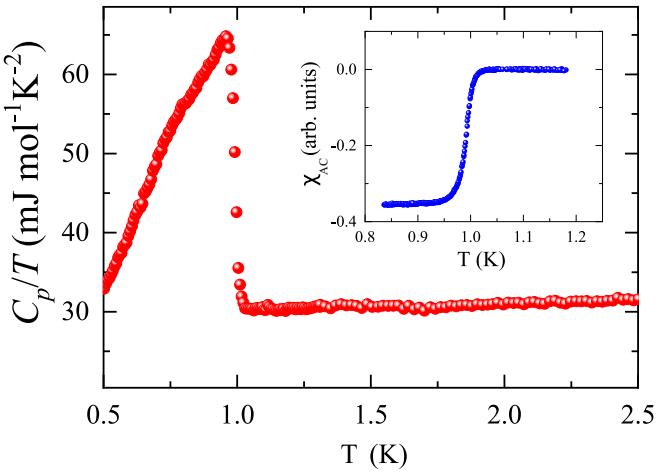

FIG. 3. Specific-heat capacity of a crystal of the isotope enriched material $^{116}Cd_2Re_2^{18}O_7$ at low temperature. The characteristic anomaly at the onset of superconducting phase at $T_c \simeq 1$ K is observed. The inset shows the AC susceptibility with a distinct drop at T_c.

Both currently known LT tetragonal space groups (phase II and phase III) are subgroups of the RT cubic space group (phase I) (see Fig. 1). The structural order parameter transforms according to the irreducible representation E_u [14,15]. The purpose of this paper is to highlight the discovery of a different noncentrosymmetric orthorhombic LT phase (phase IV in Fig. 1, space group $F222$, No. 22) for which we find strong evidence both from detailed temperature-dependent Raman scattering and from density-functional theory (DFT) calculations of the phonon dispersions (discussed below).

The paper is organized as follows. We begin with the experimental results where the Raman spectra reported in Sec. II support the existence of a different low-temperature phase (phase IV). The theory (DFT calculations) presented in Sec. III predicts the phase IV presented in Sec. III. We show that the low-temperature phase III, commonly believed to support superconductivity, is dynamically unstable and contains soft modes, whereas in contrast phase IV is stable. A short summary and conclusions are presented in Sec. IV.

II. EXPERIMENT

A. Sample preparation and characterization

Crystals of CRO with both natural isotope abundance (n-CRO) and oxygen-18 and cadmium-116 isotope substitution (i-CRO) have been prepared by chemical vapor transport [16]. All handling of the charges was carried out in a water- and oxygen-free glove box, ensuring almost complete ^{18}O substitution in the final product. This was confirmed by measuring the shift in the frequency of oxygen phonon modes [16]. Heat capacity measurements on i-CRO crystals showed a clear λ-type anomaly at the SPT from phase I to phase II at ∼204 K and a very faint anomaly at ∼114 K (see Fig. 2), indicating the SPT from phase II to phase III (see Fig. 1), in good agreement with earlier reports [11].

Figure 3 displays the heat capacity measured on a crystal of i-CRO at low temperatures. The SC transition at $T_c \sim 1$ K is clearly seen in the heat capacity and AC-susceptibility data.

B. Raman spectra

Stokes Raman scattering measurements were performed in backscattering geometry using the 632.8-nm line of a helium-neon laser at $T \in (5, 300)$ K. In preceding runs LT spectra at various laser powers (see Fig. 4) were collected and analyzed and the laser power was subsequently chosen such to evade possible laser heating effects. The measurements were carried out on the natural growth plane (111). The mode assignment by the various polarization configurations was previously published [17].

When collecting the Raman spectra we noticed a significant dependence of the spectra on the laser power. Figure 4 displays a series of spectra as a function of the laser power collected at a stabilized cryostat temperature of 29 K for a

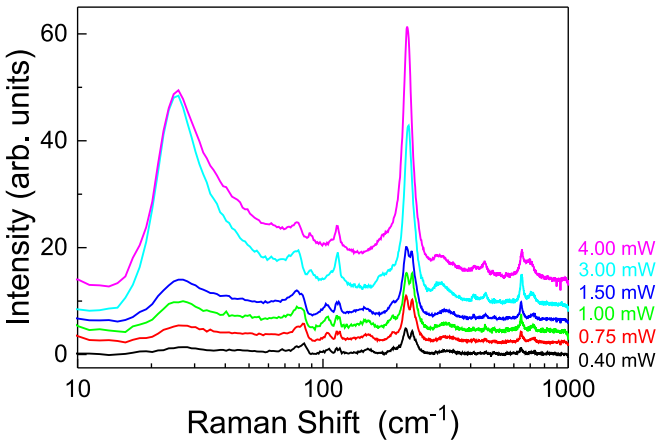

FIG. 4. Raman intensity as a function of the Raman shift of $Cd_2Re_2O_7$ (all isotope natural abundance) and increasing laser power as indicated (laser focused to a spot of 10 μm diameter) at a cryostat temperature held at 29 K. The spectra were collected on a (111) face with the polarization of the laser light and analyzer in crossed configuration. For clarity, the spectra have been vertically offset.

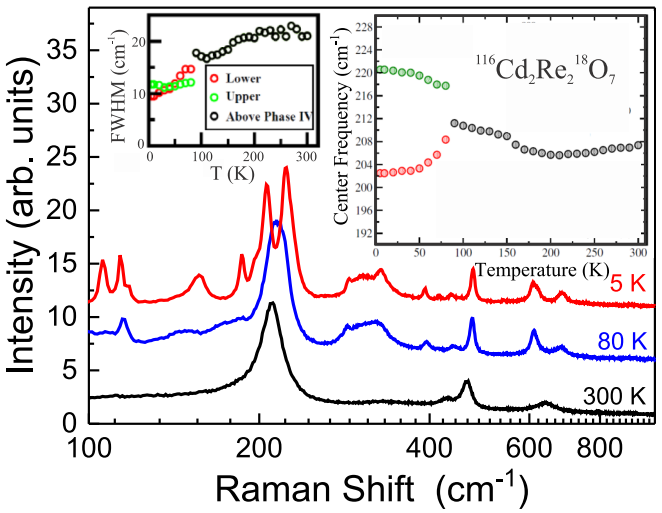

FIG. 5. Raman spectra collected without polarization analysis on a crystal of $^{116}Cd_2Re_2{}^{18}O_7$. Note the splitting below ~80 K. The right inset displays the temperature variation of the central frequencies of the 210 cm^{-1} modes obtained from a fit assuming Lorentzian profiles. The FWHMs of the modes vary between 10 and 20 cm^{-1} (see the left inset).

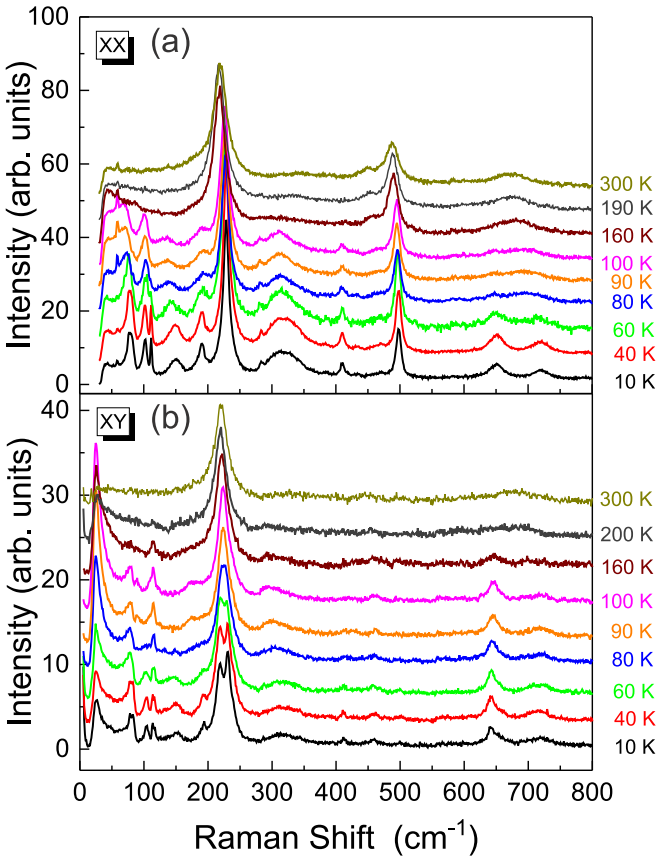

FIG. 6. Compilation of Raman spectra measured on a (111) surface of a crystal $Cd_2Re_2O_7$ (with natural isotope abundance) at various temperatures as indicated, collected with (a) parallel XX polarization and (b) cross XY polarization. The spectra have been vertically offset.

crystal of $Cd_2Re_2O_7$ with natural isotope abundance in XY cross-polarized scattering geometry. Above 1.5 mW significant spot heating leads to the disappearance of the splitting of the 220 cm^{-1} mode and the recovery of the low-frequency B_1 mode. To avoid spot heating, all further measurements were carried out with a laser power of 1 mW at a spot size of 10 μm diameter.

Representative spectra are shown in Fig. 5 for i-CRO. A downshift of all modes was observed if oxygen with the natural isotope abundance was replaced by the isotope ^{18}O (not shown). As the strongest modes in parallel configuration, we observed the A_{1g} mode at ~500 cm^{-1} with a shoulder which has been ascribed to the F_{2g} mode and the mode at 220 cm^{-1} identified as the $F_{2g} + E_g$ mode [18]. The A_{1g} mode at ~500 cm^{-1} and the broad feature between 300 and 400 cm^{-1} were observed more clearly at LT.

The main difference between the temperature dependence of our spectra of i-CRO and those of n-CRO published in the literature [17–19] is the mode splitting near 210 cm^{-1}. Its temperature dependence, shown in the right inset, and that of the FWHM (left inset) have been obtained by fitting the spectra to model Lorentzians. At temperatures $T > 200$ K, i.e., above the cubic to tetragonal SPT, we observe a slight softening of the center frequency of the mode with decreasing temperature. Below the SPT at 200 K, the mode begins to harden as the temperature is lowered, followed by the splitting with onset near 80 K. The splitting reaches 18 cm^{-1} at the lowest temperatures (see the right inset in Fig. 5).

The evolution of the Raman spectra taken for both XX and XY polarization is shown in Fig. 6. Whereas the SPT at ~200 K leads to pronounced anomalies, e.g., in the specific heat, the electrical resistivity, the Pauli susceptibility, or the thermal expansion, the SPT at ~120 K is barely perceivable in the bulk properties [20,21]. A hysteresis in the electrical resistivity points to a first-order SPT [11,20]. The impact of the SPT on the electronic band structure of CRO has been studied within DFT [22–24]. A semimetallic band structure with heavy electron bands near E_F, heavy hole bands near the zone boundary, and relatively light electron pockets around the Γ point was found. The states near E_F are sensitive to spin-orbit coupling but not to on-site Coulomb interaction at Re ions. The SPTs markedly change the carrier density near E_F, as observed in an inversion of the Hall coefficient and rapid decrease of the spin susceptibility below ~200 K [24,25].

The structural distortions induced by the SPTs of CRO are difficult to detect by x-ray or neutron scattering techniques [11]. Raman scattering experiments therefore played a central role here and were also employed to elucidate the lattice dynamical properties and the role of electron-phonon coupling [26]. Below the SPT at ~200 K, Kendziora *et al.* [17] observed a peak at zero frequency (which they ascribed to a B_1 Goldstone-mode excitation) as well as a low-frequency phonon of A_1 symmetry which they attributed to a soft mode associated with the cubic to tetragonal SPT. The latter interpretation has been questioned by Harter *et al.* [27], who argued that the apparent decrease in the Raman center frequency as the temperature of the SPT is approached from below could be due to a reduction of the phonon lifetime in

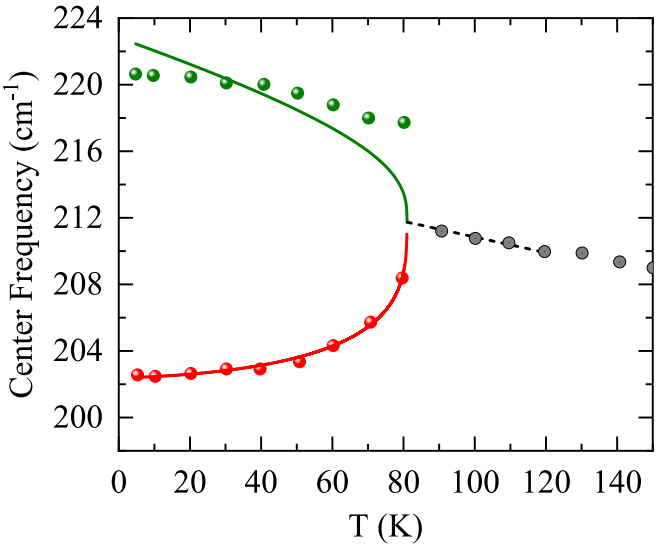

FIG. 7. Splitting of the mode observed near 210 cm^{-1} in $^{116}Cd_2Re_2^{18}O_7$ versus temperature. The solid lines represent fits of the center frequencies with a critical power law (see the text) indicating a transition temperature of ∼81 K.

agreement with the time-resolved optical reflectivity. It was proposed that multipolar nematic order rather than a structural distortion drives the inversion symmetry breaking [28].

The phonon spectra have also been studied by IR and ultrafast coherent phonon spectroscopy [27,29,30]. Optical conductivity studies revealed that the LT CRO is quite different from a simple metal [29] and exhibits anomalous Fermi liquid behavior at LT [31]. Evidence for strong electron-phonon coupling and enhanced quasiparticle damping possibly related to a SPT within the SC region was also found from an analysis of the optical conductivity [30] and the Andreev reflection [32].

C. Mode splitting below 80 K

Whereas the lower branch Raman shifts fit nicely to a critical power law, indicating a continuous SPT as predicted by the DFT results discussed below, the transition to the upper branch is steeper (see Fig. 7). Although not reporting a full splitting of this mode, the data of Bae *et al.* [19] and Knee *et al.* [18] exhibit a shoulder and weak modes at the low-energy side of the 220 cm^{-1} mode.

To investigate whether the splitting below 80 K exists not only in i-CRO, we reexamined the temperature dependence of the polarized Raman spectrum of n-CRO. Our results for n-CRO with XX and XY polarization are shown for an incident laser power of 1 mW for selected temperatures in Fig. 6. We found that there is indeed splitting of this mode observed below 80 K in the XY scattering configuration; however, utilizing too high a laser power caused the splitting to disappear (see Fig. 4). The transition to the tetragonal $I\bar{4}m2$ phase below 200 K results in other significant changes of the phonon spectrum, including a splitting of the mode near 670 cm^{-1} and additional modes appearing below 150 cm^{-1}. This observation is consistent with the prediction of a number of additional Raman active modes according to the factor group analysis [30,31].

Most prominent however is the splitting of the 220 cm^{-1} mode seen below ∼80 K in the cross-polarization configuration, which we ascribe to the additional SPT (from phase III to IV), predicted by our DFT calculations (discussed below). Its transition temperature lies clearly below the SPT from phase II to phase III (see Fig. 1). The splitting of the 220 cm^{-1} mode reflects the symmetry reduction induced by the SPT. The SPT from phase III to phase IV leads to eight different oxygen sites in a unit cell (see Table I). In addition to the remarkable splitting of the 220 cm^{-1} mode below 80 K, we also observe the splitting of the weak modes just above 100 cm^{-1}, being very pronounced in the spectra collected in a parallel configuration [Fig. 6(a)] but also seen in cross-polarization configuration [Fig. 6(b)].

III. THEORY

A. Details of DFT calculations

To provide complementary information to the Raman scattering experiments, we investigated the phonon modes in all the phases shown in Fig. 1 by DFT calculations. Our DFT calculations were performed using the projector augmented-wave method [33,34], within the generalized gradient approximation [35], implemented in the VASP program package [36]. A **k** mesh of $4 \times 4 \times 4$ points in the Monkhorst-Pack scheme was used for integration in the reciprocal space and an energy cutoff for the plane-wave expansion of 500 eV was applied. The lattice constants as well as the atom positions were optimized within the supercells of 88 atoms, employing the conjugate gradient technique and energy convergence criterion of 10^{-8} (10^{-6}) eV for electronic (ionic) iterations. The phonon dispersions and phonon densities of states (PDOSs) are shown in Fig. 8 for the possible structures of CRO, as calculated using the direct method [37] implemented in the PHONON software [38]. Since the number of atoms in the primitive cells is 22, one finds 66 phonon modes in each phase.

B. Structural data

In Table I we summarize the structural data as obtained from experiment [24] and from the present DFT calculations: a, b, and c denote the lattice parameters, while a', b', and c' denote the sizes of the supercell used for the calculations; V (V') is the volume of the unit cell (supercell). We have included also the total energies given per one supercell with 88 atoms for all studied phases.

The calculated lattice parameters are slightly overestimated when compared to the experimental data obtained for the three known phases of $Cd_2Re_2O_7$. Such an increase of lattice parameters is typical for calculations performed within the generalized gradient approximation approach. Note that for phase I and phase IV, the unit cell and the supercell used for calculation are the same, whereas for phase II and phase III the size (volume) of the supercells is twice larger than for the unit cells. This ensures that not only the number of atoms in each supercell is the same for all considered phases, but also the size of supercell is large enough to perform phonon calculations. In each phase there is a different number of inequivalent positions of oxygen atoms.

TABLE I. Lattice parameters and atomic positions in the crystal structures I–III of $Cd_2Re_2O_7$ (Fig. 1), as obtained from experiment [24] and from the DFT calculations (see Sec. III A). Total energies E are calculated with respect to phase I, $E_{\rm I} = 0$. The parameters for the experimental data are (a) $a = b = c = 10.2261(5)$ Å, (b) $a = b = 7.2312(3)$ Å and $c = 10.2257(4)$ Å, and (c) $a = b = 7.2313(3)$ Å and $c = 10.2282(6)$ Å. The parameters for the DFT calculations are: (a) $V_{\rm I} = 1118.90$ Å^3, $E_{\rm I} = 0$, and $a = b = c = 10.3816$ Å; (b) $V'_{\rm II} = 1122.31$ Å^3, $E_{\rm II} = -2.08510$ eV, $a = b = 7.3420$ Å, $c = 10.4101$ Å, $a' = b' = 10.3831$ Å ($a' = \sqrt{2}a$), and $c' = 10.4101$ Å; and (c) $V'_{\rm III} = 1121.87$ Å^3, $E_{\rm III} = -2.02515$ eV, $a = b = 7.3537$ Å, $c = 10.3729$ Å, $a' = b' = 10.3997$ Å ($a' = \sqrt{2}a$), and $c' = 10.3729$ Å.

Experimental data [24]				DFT calculations			
Atom	x	y	z	Atom	x	y	z
			(a) Phase I: $Fd\bar{3}m$ (227)				
Re	0.2500	0.7500	0.5000	Re	0.0000	0.2500	0.2500
Cd	0.5000	0.5000	0.5000	Cd	0.5000	0.5000	0.5000
O(1)	0.3152(9)	0.6250	0.6250	O(1)	0.3141	0.1250	0.1250
O(2)	0.6250	0.6250	0.6250	O(2)	0.6250	0.6250	0.6250
			(b) Phase II: $I\bar{4}m2$ (119)				
Re	0.2471(2)	0.0000	0.87294(15)	Re	0.2510	0.0000	0.8760
Cd	0.0000	0.2471(5)	0.6259(3)	Cd	0.0000	0.2372	0.6386
O(1)	0.3059(15)	0.1941(15)	0.7500	O(1)	0.3000	0.2000	0.7500
O(2)	0.0000	0.0000	0.8026(16)	O(2)	0.0000	0.0000	0.7947
O(3)	0.1889(16)	0.1889(16)	0.0000	O(3)	0.1795	0.1795	0.0000
O(4)	0.5000	0.0000	0.9317(19)	O(4)	0.5000	0.0000	0.9189
O(5)	0.0000	0.0000	0.5000	O(5)	0.0000	0.0000	0.5000
O(6)	0.0000	0.5000	0.7500	O(6)	0.0000	0.5000	0.7500
			(c) Phase III: $I4_122$ (98)				
Re	0.2500	0.9967(3)	0.8750	Re	0.2500	0.0020	0.8750
Cd	0.5041(6)	0.2500	0.1250	Cd	0.5229	0.2500	0.1250
O(1)	0.1880(20)	0.1880(20)	0.0000	O(1)	0.1711	0.1711	0.0000
O(2)	0.5000	0.0000	0.9396(14)	O(2)	0.5000	0.0000	0.9424
O(3)	0.1970(20)	0.8030(20)	0.0000	O(3)	0.2032	0.7968	0.0000
O(4)	0.5000	0.5000	0.0000	O(4)	0.5000	0.5000	0.0000

In Table II we give the predictions from the theory for the lattice parameters, atomic positions, and total energy in phase IV of $Cd_2Re_2O_7$. This phase is predicted by the DFT calculations and has stable phonon modes (see Sec. III C). The symmetry of this phase predicted from the theory is $F222$.

TABLE II. Lattice parameters and atomic positions in the crystal structure of $Cd_2Re_2O_7$ at low temperature in phase IV: $F222$ (22) found from DFT calculations. The other parameters are $V_{\rm IV} = 1122.28$ Å^3, $E_{\rm IV} = -2.08515$ eV, $a = 10.3832$ Å, $b = 10.3828$ Å, and $c = 10.4102$ Å. Total energy $E_{\rm IV}$ is given with respect to phase I, $E_{\rm I} = 0$ (see Table I).

Atom	x	y	z
Re	0.1245	0.1245	0.1260
Cd	0.6314	0.6314	0.6114
O(1)	0.5000	0.5000	0.1689
O(2)	0.0706	0.2500	0.2500
O(3)	0.2500	0.4295	0.2500
O(4)	0.5000	0.2000	0.5000
O(5)	0.2000	0.5000	0.5000
O(6)	0.2500	0.2500	0.0447
O(7)	0.5000	0.5000	0.5000
O(8)	0.7500	0.7500	0.7500

C. Phonon instabilities in phases I and III

The phonon spectra in phase I and phase III exhibit imaginary (soft) modes, indicating that these phases are dynamically unstable at $T = 0$. The most unstable is the cubic structure (phase I). The lowest-energy soft phonon is a doubly degenerate mode with the irreducible representation E_u, which agrees with the group theory analysis [14] and the previous DFT study [15]. This indicates the displacive character of the phase I to phase II SPT connected with the soft mode, although one cannot rule out a more complex mechanism involving electron-phonon interactions. Regardless of the mechanism of the SPT, our calculations show that the total energy of the tetragonal phase II is lowered by -2.085 eV and it is dynamically stable.

Surprisingly, in the tetragonal phase III we found (again) the soft modes close to the Γ point. The irreducible representation of the lowest imaginary mode is here B_2. Group theory analysis shows that this mode breaks tetragonal symmetry and generates the orthorhombic noncentrosymmetric structure (space group $F222$), called phase IV. We obtained its crystal structure using the polarization vectors of the B_2 soft mode and optimized its crystal structure parameters (see Sec. III B). The orthorhombic distortion is very weak with the difference between the a and b lattice parameters about 0.004%. The total energy of this structure is lower than that of the tetragonal phase III by -0.06 eV. The energy difference between phases II and IV is much smaller (-0.05 meV) without zero-point

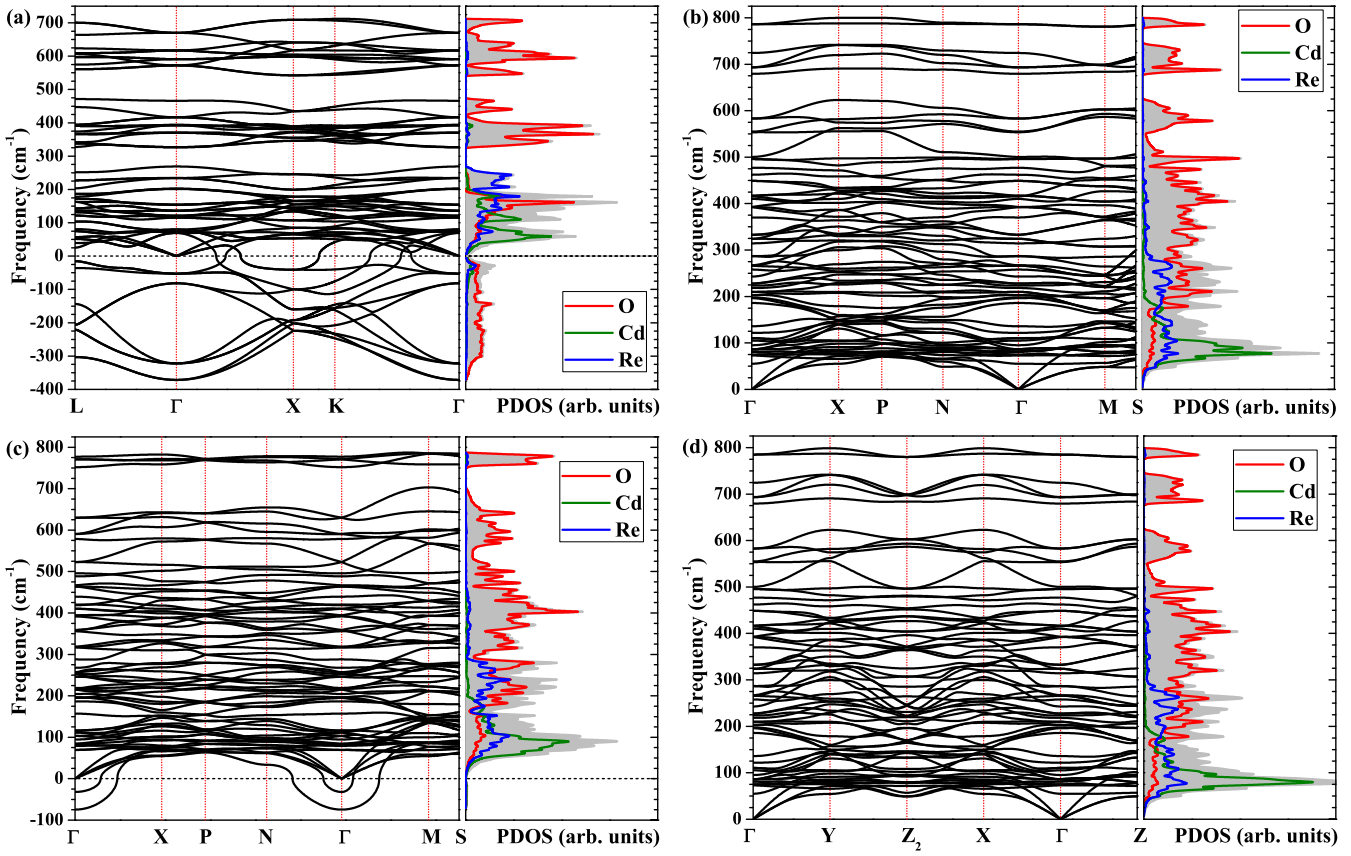

FIG. 8. Phonon dispersion curves (the left of every panel) and PDOSs (the right of every panel) for each phase: (a) $Fd\bar{3}m$ phase I, (b) $I\bar{4}m2$ phase II, (c) $I4_122$ phase III, and (d) $F222$ phase IV. Stable phases are II and IV. The gray shaded areas represent the total PDOSs on the right, while the partial PDOSs due to vibrations of O, Cd, and Re atoms are shown by red, green, and blue lines, respectively.

energies. After including them, the energy difference between phases II and IV equals -2.069 meV, which shows that phase IV is mainly stabilized by quantum fluctuations. This phase is stable and has only real phonon modes [see Fig. 8(d)].

The contribution of particular atoms to the phonon spectra can be analyzed using the PDOSs (see Fig. 8). The Cd (Re) atoms vibrate mainly with frequencies below 200 cm^{-1} [$\omega \in (0, 300)$ cm^{-1}]. Above 300 cm^{-1} oxygen vibrations dominate with the cutoff around 700 (800) cm^{-1} in the cubic (tetragonal) structure. The soft modes found in the cubic phase largely contribute to the PDOSs with the dominant component of oxygen vibrations, but have negligible weight in the PDOSs in the $I4_122$ tetragonal phase.

D. Influence of isotope substitution and quantum fluctuations on phase transitions

We remark that the SC transition temperature T_c of CRO shows an oxygen isotope effect, $\alpha_{SC} = -(d \ln T_c / d \ln m)$, which amounts to less than 0.05(1). Such a weak isotope effect indicates that another pairing mechanism different from phonons may contribute to the onset of superconductivity, similar to high-T_c superconductors [39]. This motivates also the search for possible contributions of triplet superconductivity, possible here due to strong spin-orbit coupling [11,28,40–42]. Raman modes associated with oxygen vibrations exhibit noticeable oxygen isotope shifts with $\alpha_\omega = -(d \ln \omega / d \ln m)$ ranging between 0.35 and 0.44, indicating substantial oxygen sensitivity of the low-energy phonons. The difference between both oxygen isotopes, i.e., between n-CRO and i-CRO, is however less pronounced than in, e.g., the ferroelectricity in $SrTiO_3$, where for crystals containing only ^{16}O isotope the transition to a ferroelectric phase is suppressed by quantum fluctuations, whereas ^{18}O substitution induces ferroelectric phases with T_c up to $\sim$25 K [43–47].

It is worth noting that we performed also phonon calculations for the i-CRO system and we did not find any qualitative differences in comparison to the n-CRO system. Only the frequencies associated with oxygen and cadmium atoms were shifted slightly to lower (absolute) values than those in n-CRO, as expected in the case of heavier atomic masses.

IV. CONCLUSION

In summary, we have presented remarkable agreement between the experimental observations and the predictions of *ab initio* phonon calculations, which indicates the existence of an orthorhombic noncentrosymmetric phase IV in $Cd_2Re_2O_7$ at $T < 80$ K. This phase is stable and should be carefully studied further to resolve the puzzles about the mechanism of exotic superconductivity in $Cd_2Re_2O_7$ [48,49]. We considered

the distinct splitting of the 220 cm^{-1} mode as strong support for the low-temperature structural phase detected as well by our DFT phonon calculations.

Recent group theory analysis [50] suggests that the low-temperature phase of $Cd_2Re_2O_7$ could be of $F222$ symmetry. Our phonon studies resolve this problem and confirm that the low-temperature phase (phase IV) has indeed $F222$ symmetry, contrary to the previous expectations. A factor group analysis for space group $F222$ using the atom positions given in Table II and the associated Wyckoff positions indeed showed that all Raman active modes are single A and B modes, whereas in phase III (space group $I4_122$) for all atoms still doubly degenerate Raman active E modes are present.

ACKNOWLEDGMENTS

The authors are grateful to Andres Greco and Krzysztof Parlinski for very insightful discussions and comments. This work was supported by Narodowe Centrum Nauki (National Science Centre, Poland) under Projects No. 2017/24/C/ST3/00276 (K.J.K.), No. 2017/25/B/ST3/02586 (A.P. and P.P.), and No. 2016/23/B/ST3/00839 (A.M.O.) as well as by the Natural Sciences and Engineering Research Council of Canada through Grants No. DDG-2017-00043 (M.R.) and No. RGPIN-2018-04438 (F.S.R.). A.M.O. is grateful for support via the Alexander von Humboldt Foundation Fellowship [51] (Humboldt-Forschungspreis).

[1] M. Smidman, M. B. Salamon, H. Q. Yuan, and D. F. Agterberg, Superconductivity and spin-orbit coupling in non-centrosymmetric materials: A review, Rep. Prog. Phys. **80**, 036501 (2017).

[2] Y. Okuda, Y. Miyauchi, Y. Ida, Y. Takeda, C. Tonohiro, Y. Oduchi, T. Yamada, N. D. Dung, T. D. Matsuda, Y. Haga, T. Takeuchi, M. Hagiwara, K. Kindo, H. Harima, K. Sugiyama, R. Settai, and Y. Onuki, Magnetic and superconducting properties of $LaIrSi_3$ and $CeIrSi_3$ with the non-centrosymmetric crystal structure, J. Phys. Soc. Jpn. **76**, 044708 (2007).

[3] Y. Yanase and M. Sigrist, Magnetic properties in non-centrosymmetric superconductors with and without antiferromagnetic order, J. Phys. Soc. Jpn. **76**, 124709 (2007); Superconductivity and magnetism in non-centrosymmetric system: Application to $CePt_3Si$, *ibid.* **77**, 124711 (2008).

[4] Y. Matsubayashi, K. Sugii, D. Hirai, Z. Hiroi, T. Hasegawa, S. Sugiura, H. T. Hirose, T. Terashima, and S. Uji, Coexistence of odd-parity and even-parity order parameters in the multipole order phase of the spin-orbit coupled metal $Cd_2Re_2O_7$, Phys. Rev. B **101**, 205133 (2020).

[5] Y. Matsubayashi, K. Sugii, H. T. Hirose, D. Hirai, S. Sugiura, T. Terashima, S. Uji, and Z. Hiroi, Split Fermi surfaces of the spin–orbit-coupled metal $Cd_2Re_2O_7$ probed by de Haas–van Alphen effect, J. Phys. Soc. Jpn. **87**, 053702 (2018).

[6] W. Witczak-Krempa, G. Chen, Y. B. Kim, and L. Balents, Correlated quantum phenomena in the strong spin-orbit regime, Annu. Rev. Condens. Matter Phys. **5**, 57 (2014).

[7] R. Schaffer, E. K.-H. Lee, B.-J. Yang, and Y. B. Kim, Recent progress on correlated electron systems with strong spin-orbit coupling, Rep. Prog. Phys. **79**, 094504 (2016).

[8] M. Hanawa, Y. Muraoka, T. Tayama, T. Sakakibara, J. Yamaura, and Z. Hiroi, Superconductivity at 1 K in $Cd_2Re_2O_7$, Phys. Rev. Lett. **87**, 187001 (2001).

[9] H. Sakai, K. Yoshimura, H. Ohno, H. Kato, S. Kambe, R. E. Walstedt, T. D. Matsuda, Y. Haga, and Y. Onuki, Superconductivity in a pyrochlore oxide $Cd_2Re_2O_7$, J. Phys.: Condens. Matter **13**, L785 (2001).

[10] R. Jin, J. He, S. McCall, C. S. Alexander, F. Drymiotis, and D. Mandrus, Superconductivity in the correlated pyrochlore $Cd_2Re_2O_7$, Phys. Rev. B **64**, 180503(R) (2001).

[11] Z. Hiroi, J.-I. Yamaura, T. C. Kobayashi, Y. Matsubayashi, and D. Hirai, Pyrochlore oxide superconductor $Cd_2Re_2O_7$ revisited, J. Phys. Soc. Jpn. **87**, 024702 (2018).

[12] J.-I. Yamaura and Z. Hiroi, Low temperature symmetry of pyrochlore oxide $Cd_2Re_2O_7$, J. Phys. Soc. Jpn. **71**, 2598 (2002).

[13] Z. Hiroi, J.-I. Yamaura, Y. Muraoka, and M. Hanawa, Second phase transition in pyrochlore oxide $Cd_2Re_2O_7$, J. Phys. Soc. Jpn. **71**, 1634 (2002).

[14] I. A. Sergienko and S. H. Curnoe, Structural order parameter in the pyrochlore superconductor $Cd_2Re_2O_7$, J. Phys. Soc. Jpn. **72**, 1607 (2003).

[15] I. A. Sergienko, V. Keppens, M. McGuire, R. Jin, J. He, S. H. Curnoe, B. C. Sales, P. Blaha, D. J. Singh, K. Schwarz, and D. Mandrus, Metallic "Ferroelectricity" in the Pyrochlore $Cd_2Re_2O_7$, Phys. Rev. Lett. **92**, 065501 (2004).

[16] F. S. Razavi, M. Hajialamdari, M. Reedyk, and R. K. Kremer, Isotope effect on superconductivity and Raman phonons of pyrochlore $Cd_2Re_2O_7$, Physica C **549**, 11 (2018).

[17] C. A. Kendziora, I. A. Sergienko, R. Jin, J. He, V. Keppens, B. C. Sales, and D. Mandrus, Goldstone-Mode Phonon Dynamics in the Pyrochlore $Cd_2Re_2O_7$, Phys. Rev. Lett. **95**, 125503 (2005).

[18] C. S. Knee, J. Holmlund, J. Andreasson, M. Käll, S. G. Eriksson, and L. Börjesson, Order-disorder-order phase transitions in the pyrochlore superconductor $Cd_2Re_2O_7$, Phys. Rev. B **71**, 214518 (2005).

[19] J. S. Bae, H. K. Ko, I.-S. Yang, Y. S. Lee, T. W. Noh, R. Jin, J. He, and D. Mandrus, Temperature-dependent Raman study of the pyrochlore superconductor $Cd_2Re_2O_7$, J. Korean Phys. Soc. **48**, 946 (2006).

[20] Z. Hiroi and M. Hanawa, Superconducting properties of the pyrochlore oxide $Cd_2Re_2O_7$, J. Phys. Chem. Solids **63**, 1021 (2002).

[21] M. Tachibana, N. Taira, H. Kawaji, and E. Takayama-Muromachi, Thermal properties of $Cd_2Re_2O_7$ and $Cd_2Nb_2O_7$ at the structural phase transitions, Phys. Rev. B **82**, 054108 (2010).

[22] D. J. Singh, P. Blaha, K. Schwarz, and J. O. Sofo, Electronic structure of the pyrochlore metals $Cd_2Os_2O_7$ and $Cd_2Re_2O_7$, Phys. Rev. B **65**, 155109 (2002).

[23] H. Harima, Electronic band structures on $5d$-transition metal pyrochlore: $Cd_2Re_2O_7$ and $Cd_2Os_2O_7$, J. Phys. Chem. Solids **63**, 1035 (2002).

[24] S.-W. Huang, H.-T. Jeng, J.-Y. Lin, W. J. Chang, J. M. Chen, G. H. Lee, H. Berger, H. D. Yang, and K. S. Liang, Electronic structure of pyrochlore $Cd_2Os_2O_7$, J. Phys.: Condens. Matter **21**, 195602 (2009).

[25] O. Vyaselev, K. Arai, K. Kobayashi, J. Yamazaki, K. Kodama, M. Takigawa, M. Hanawa, and Z. Hiroi, Superconductivity and Magnetic Fluctuations in $Cd_2Re_2O_7$ via Cd Nuclear Magnetic Resonance and Re Nuclear Quadrupole Resonance, Phys. Rev. Lett. **89**, 017001 (2002).

[26] Y. Matsubayashi, T. Hasegawa, N. Ogita, J.-I. Yamaura, and Z. Hiroi, High-pressure Raman study on the superconducting pyrochlore oxide $Cd_2Re_2O_7$, Physica B **536**, 600 (2018).

[27] J. W. Harter, D. M. Kennes, H. Chu, A. de la Torre, Z. Y. Zhao, J.-Q. Yan, D. G. Mandrus, A. J. Millis, and D. Hsieh, Evidence of an Improper Displacive Phase Transition in $Cd_2Re_2O_7$ via Time-Resolved Coherent Phonon Spectroscopy, Phys. Rev. Lett. **120**, 047601 (2018).

[28] J. W. Harter, Z. Y. Zhao, J.-Q. Yan, D. G. Mandrus, and D. Hsieh, A parity-breaking electronic nematic phase transition in the spin-orbit coupled metal $Cd_2Re_2O_7$, Science **356**, 295 (2017).

[29] N. L. Wang, J. J. McGuire, T. Timusk, R. Jin, J. He, and D. Mandrus, Optical evidence for mass enhancement of quasiparticles in pyrochlore $Cd_2Re_2O_7$, Phys. Rev. B **66**, 014534 (2002).

[30] M. Hajialamdari, F. S. Razavi, D. A. Crandles, R. K. Kremer, and M. Reedyk, Far-IR excitations in $Cd_2Re_2O_7$ in the normal and superconducting states, J. Phys.: Condens. Matter **24**, 505701 (2012).

[31] M. Hajialamdari, F. S. Razavi, and M. Reedyk, Anomalous Fermi liquid state in pyrochlore heavy electron superconductor $Cd_2Re_2O_7$, Physica B **502**, 170 (2016).

[32] F. S. Razavi, Y. Rohanizadegan, M. Hajialamdari, M. Reedyk, R. K. Kremer, and B. Mitrović, The effect of quasiparticle self-energy on $Cd_2Re_2O_7$ superconductor, Can. J. Phys. **93**, 1646 (2015).

[33] P. E. Blöchl, Projector augmented-wave method, Phys. Rev. B **50**, 17953 (1994).

[34] G. Kresse and D. Joubert, From ultrasoft pseudopotentials to the projector augmented-wave method, Phys. Rev. B **59**, 1758 (1999).

[35] J. P. Perdew, K. Burke, and M. Ernzerhof, Generalized Gradient Approximation Made Simple, Phys. Rev. Lett. **77**, 3865 (1996); Generalized Gradient Approximation Made Simple [Phys. Rev. Lett. **77**, 3865 (1996)], **78**, 1396(E) (1997).

[36] G. Kresse and J. Furthmüller, Efficient iterative schemes for *ab initio* total-energy calculations using a plane-wave basis set, Phys. Rev. B **54**, 11169 (1996); Efficiency of ab-initio total energy calculations for metals and semiconductors using a plane-wave basis set, Comput. Mater. Sci. **6**, 15 (1996).

[37] K. Parlinski, Z. Q. Li, and Y. Kawazoe, First-Principles Determination of the Soft Mode in Cubic ZrO_2, Phys. Rev. Lett. **78**, 4063 (1997).

[38] K. Parlinski, PHONON, version 6.15 (Computing for Materials, Cracow, 2015).

[39] D. Zech, H. Keller, K. Conder, E. Kaldis, E. Liarokapis, N. Poulakis, and K. A. Müller, Site-selective oxygen isotope effect in optimally doped $YBa_2Cu_3O_{6+x}$, Nature (London) **371**, 681 (1994).

[40] L. Fu, Parity-Breaking Phases of Spin-Orbit-Coupled Metals with Gyrotropic, Ferroelectric, and Multipolar Orders, Phys. Rev. Lett. **115**, 026401 (2015).

[41] J. Yamaura, K. Takeda, Y. Ikeda, N. Hirao, Y. Ohishi, T. C. Kobayashi, and Z. Hiroi, Successive spatial symmetry breaking under high pressure in the spin-orbit-coupled metal $Cd_2Re_2O_7$, Phys. Rev. B **95**, 020102(R) (2017).

[42] S. Hayami, Y. Yanagi, H. Kusunose, and Y. Motome, Electric Toroidal Quadrupoles in the Spin-Orbit-Coupled Metal $Cd_2Re_2O_7$, Phys. Rev. Lett. **122**, 147602 (2019).

[43] M. Itoh, R. Wang, Y. Inaguma, T. Yamaguchi, Y.-J. Shan, and T. Nakamura, Ferroelectricity Induced by Oxygen Isotope Exchange in Strontium Titanate Perovskite, Phys. Rev. Lett. **82**, 3540 (1999).

[44] A. Bussmann-Holder, H. Büttner, and A. R. Bishop, Stabilization of ferroelectricity in quantum paraelectrics by isotopic substitution, J. Phys.: Condens. Matter **12**, L115 (2000); Polar-Soft-Mode-Driven Structural Phase Transition in $SrTiO_3$, Phys. Rev. Lett. **99**, 167603 (2007).

[45] Y. Yamada, N. Todoroki, and S. Miyashita, Theory of ferroelectric phase transition in $SrTiO_3$ induced by isotope replacement, Phys. Rev. B **69**, 024103 (2004).

[46] S. E. Rowley, L. J. Spalek, R. P. Smith, M. P. M. Dean, M. Itoh, J. F. Scott, G. G. Lonzarich, and S. S. Saxena, Quantum criticality in ferroelectrics, Nat. Phys. **10**, 367 (2014).

[47] J. M. Edge, Y. Kedem, U. Aschauer, N. A. Spaldin, and A. V. Balatsky, Quantum Critical Origin of the Superconducting Dome in $SrTiO_3$, Phys. Rev. Lett. **115**, 247002 (2015).

[48] J. Ruhman, V. Kozii, and L. Fu, Odd-Parity Superconductivity near an Inversion Breaking Quantum Critical Point in One Dimension, Phys. Rev. Lett. **118**, 227001 (2017).

[49] S. Di Matteo and M. R. Norman, Nature of the tensor order in $Cd_2Re_2O_7$, Phys. Rev. B **96**, 115156 (2017).

[50] M. R. Norman, Crystal structure of the inversion-breaking metal $Cd_2Re_2O_7$, Phys. Rev. B **101**, 045117 (2020).

[51] https://www.humboldt-foundation.de/web/humboldt-preis.html.